Research in Astronomy and Astrophysics, 25:035013 (10pp), 2025 March
https://doi.org/10.1088/1674-4527/adb896
CSTR: 32081.14.RAA.adb896

Four Total Eclipsing Contact Binary Systems: The First Photometric Light Curve Solutions Employing TESS and Gaia Surveys

Atila Poro[1,2], Razieh Aliakbari[3], Hossein Azarara[4], Asma Ababafi[5], and Sadegh Nasirian[6]
[1] LUX, Observatoire de Paris, CNRS, PSL, 61 Avenue de l'Observatoire, 75014 Paris, France; atila.poro@obspm.fr
[2] Astronomy Department of the Raderon AI Lab, Burnaby, BC., Canada
[3] Physics Society of Iran (PSI), Tehran, Iran
[4] Physics Department, Shahid Bahonar University of Kerman, Kerman, Iran
[5] Independent Astrophysics Researcher, Dezful, Iran
[6] Thaqib Astronomical Association, Rasht, Iran
Received 2024 December 31; revised 2025 January 24; accepted 2025 February 19; published 2025 March 14

Abstract

We presented the first photometric light curve solutions of four W Ursae Majoris-type contact binary systems. This investigation utilized photometric data from the Transiting Exoplanet Survey Satellite and Gaia Data Release 3 (DR3). We used the PHysics Of Eclipsing BinariEs Python code and the Markov Chain Monte Carlo method for these light curve solutions. Only TIC 249064185 among the target systems needed a cold starspot to be included in the analysis. Based on the estimated mass ratios for these total eclipse systems, three of them are categorized as low mass ratio contact binary stars. The absolute parameters of the systems were estimated using the Gaia DR3 parallax method and the orbital period and semimajor axis (P–a) empirical relationship. We ascertained that the TIC 318015356 and TIC 55522736 systems are A-subtypes, while TIC 249064185 and TIC 397984843 are W-subtypes, depending on each component's effective temperature and mass. We estimated the initial masses of the stars, the mass lost by the binary system, and the systems' ages. We displayed star positions in the mass–radius, mass–luminosity, and total mass–orbital angular momentum diagrams. In addition, our findings indicate a good agreement with the mass-temperature empirical parameter relationship for the primary stars.

Key words: (stars:) binaries (including multiple): close – stars: fundamental parameters – methods: data analysis

1. Introduction

The W Ursae Majoris (W UMa)-type eclipsing contact binary systems have two late-type stars with a short orbital period. The two components in the system overfill their respective critical Roche lobes and share a common envelope (Kopal 1959).

Contact binaries are generally classified into two subtypes, A and W (Binnendijk 1970). The subtype of a system can be recognized by estimating its temperatures and the masses of the stars.

The contact systems' stars are transferring mass and energy to each other (Lucy & Wilson 1979), and their orbital period changes in this process. The orbital period of contact systems plays a role in studying empirical relationships of the fundamental parameters and is effective in the evolutionary process of these systems (Lazarević et al. 2021; Loukaidou et al. 2022). There are studies conducted on the upper and lower cut-offs of these systems' orbital periods (Zhang & Qian 2020). The investigations show that contact systems' orbital periods usually lie between about 0.2 and 0.6 days (Poro et al. 2024e).

The asymmetric light curves in contact and near-contact binaries are commonly observed in phases 0.25 and 0.75. This phenomenon is generally referred to as the O'Connell effect (O'Connell 1951), which is crucial for studying a star's magnetic activity. This asymmetry in the light curves is solved with one or more starspot(s).

In recent decades, surveys such as Kepler (Borucki et al. 2010), the Catalina Sky Survey (Marsh et al. 2017), the All-Sky Automated Survey for Supernovae (ASAS-SN; Jayasinghe et al. 2018), the Asteroid Terrestrial-impact Last Alert System (Heinze et al. 2018), and the Transiting Exoplanet Survey Satellite (TESS) mission (Ricker et al. 2015) have contributed to a dramatic rise in the number of known eclipsing contact binaries. Our knowledge of W UMa stars is still incomplete, even with this previous improvement. Light curve modeling, mass ratio estimation, and component temperature enable the determination of the absolute stellar parameters: the masses, radii, and brightnesses of the components in solar units (Kallrath & Milone 1999). Also, increasing the number of well-studied W UMa binaries with absolute parameters enables astronomers to derive empirical parameter relationships.

In this investigation, we present a photometric analysis for four contact binary systems. The paper is organized as follows: Section 2 provides specifications of the target systems and the data set. Section 3 contains the light curve solution for the

Table 1
Specifications of the Target Systems

Name TIC	Name Gaia DR3	R.A.° (J2000)	Decl.° (J2000)	d (pc)	P_0 (day)	t_0 (BJD_{TDB})
249064185	3208726533053539072	79.260986	−5.263103	744(22)	0.3501901	2457700.651071
318015356	2992215135718505984	90.045663	−15.829143	644(6)	0.4169211	2458037.850993
397984843	534022116032892032	23.410532	71.043707	1155(19)	0.4576875	2458028.072765
55522736	5543014496502562432	126.173182	−35.458112	1071(15)	0.3897012	2458205.512582

Table 2
Specifications of the Target Systems from TESS

System	V (mag.)	Sector	Exposure Length (s)	Observation Start
TIC 249064185	13.626(149)	32	600	2020
TIC 318015356	11.870(22)	33	600	2020
TIC 397984843	14.151(149)	58	200	2022
TIC 55522736	13.728(114)	62	200	2023

system. Section 4 presents the estimation of the absolute parameters. Finally, Section 5 includes the discussion and conclusion.

2. Target Systems and Data Set

For this investigation, four contact binary stars were chosen, including TIC 249064185, TIC 318015356, TIC 397984843, and TIC 55522736. According to the appearance of their light curves, these systems exhibited total eclipses, but in-depth photometric analysis has not yet been performed on them. The target systems are all categorized as contact binary stars in several catalogs, such as the ASAS-SN (Jayasinghe et al. 2018), ZTF[7] (Chen et al. 2020), GCVS[8] (Samus' et al. 2017), APASS DR9[9] (Henden et al. 2015), and VSX[10] catalogs. The general characteristics of the targets are presented in Table 1 including the names of the systems in two catalogs, coordinates and distances from the Gaia Data Release 3 (DR3) database, and reference ephemerides including orbital period P_0 and minimum time t_0 from the literature. We utilized the online tool[11] to convert the Heliocentric Julian Date (HJD) to the Barycentric Julian Date (BJD_{TDB}) since t_0 was reported in HJD.

We used TESS data to analyze these systems. TESS has a time series and good-quality data for each target system. The TESS data were obtained from the database of the Mikulski Archive for Space Telescopes (MAST).[12] TESS-style curves were extracted from the MAST using the LightKurve[13] code. The data were detrended using the TESS Science Processing Operations Center pipeline (Jenkins et al. 2016). We selected systems' light curves based on the most recent or better-quality observed TESS sector that was available. The characteristics of the observations and sectors used in this study of TESS are listed in Table 2. The apparent magnitude (V) of the systems in Table 2 is from the TESS Input Catalog (TIC) v8.2 database.

We also used Gaia space-based telescope data for this study. Time-series photometric data were accessed through the online service provided by the Gaia team at the Astronomisches Rechen-Institut.[14] The data were downloaded in VOTable format, a standard file format used in the Virtual Observatory, and analyzed using TOPCAT (Taylor 2005). We extracted Gaia's G photometric filter data.

3. Light Curve Solutions

The light curves of the contact systems were analyzed using the PHysics Of Eclipsing BinariEs (PHOEBE) Python code version 2.4.9 (Prša et al. 2016; Conroy et al. 2020). We also made use of the BSN application.[15] The four target binary systems' light curves were investigated for the first time. The short orbital period and the type described in the catalogs led us to choose a contact mode, however, the light curves of each system exhibited the eclipsing contact binary features. It was assumed that the bolometric albedo was $A_1 = A_2 = 0.5$ (Ruciński 1969) and that the gravity-darkening coefficients were $g_1 = g_2 = 0.32$ (Lucy 1967). The PHOEBE code provided the limb darkening coefficients as a free parameter, and the

[7] Zwicky Transient Facility.
[8] General Catalogue of Variable Stars.
[9] AAVSO Photometric All-Sky Survey.
[10] Variable Star Index, https://www.aavso.org/vsx/.
[11] https://astroutils.astronomy.osu.edu/time/hjd2bjd.html
[12] https://mast.stsci.edu/portal/Mashup/Clients/Mast/Portal.htmL
[13] https://docs.lightkurve.org
[14] https://gaia.ari.uni-heidelberg.de
[15] https://bsnp.info/

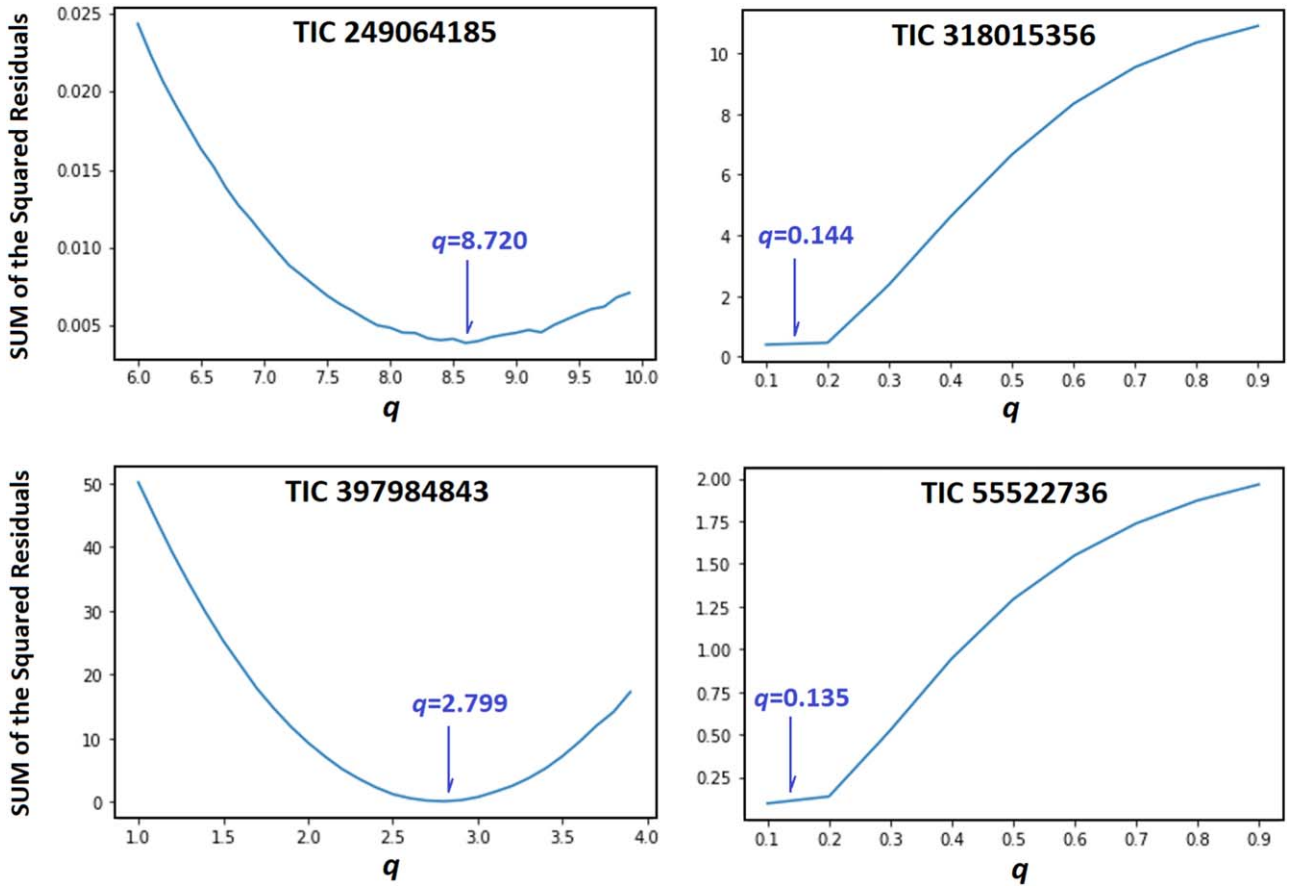

Figure 1. Sum of the squared residuals as a function of the mass ratio.

stellar atmosphere was modeled using the Castelli & Kurucz (2004) study.

We set the effective temperature of the hotter stars using the temperature reported by Gaia DR3.[16] The effective temperature set on the hotter star is close to the value obtained by the orbital period-effective temperature (P–T_1) relationship presented by the Lazarević et al. (2021) study. Comparing the final effective temperatures of the hotter stars to the Gaia DR3 values, they are in an acceptable range (Poro et al. 2025).

We obtained the mass ratio (q) of the systems by using the q-search in the photometric data. We searched a range of mass ratios between $q = 0.1$ and $q = 10$. Then, we shortened the interval and searched again according to the minimum sum of squared residuals. Figure 1 displays the q-search results for four systems. The q-search curves display a sharp bottom, which allows the determination of an acceptable mass ratio for these total eclipsing contact systems (Li et al. 2021; Poro et al. 2024d).

The well-known O'Connell effect is indicated by the asymmetry in the brightness of maximums in the light curve of eclipsing binary stars (O'Connell 1951; Sriram et al. 2017). One explanation for this phenomenon could be the existence of starspot(s) due to magnetic activity on the star's surface.

We used PHOEBE's optimization tool to improve the output of the light curve solutions to yield the initial results. The final values of the parameters and their uncertainty were obtained using the Markov Chain Monte Carlo (MCMC) approach based on the emcee package (Foreman-Mackey et al. 2013). Therefore, five main parameters, including i, q, f, and $T_{1,2}$, were considered for the MCMC modeling process. We selected the Gaussian distribution that adequately encompasses the entire observational light curve and employed 36 walkers and 1500 iterations for target systems. According to the light curve solutions, no target system showed a third body (l_3).

Table 3 presents the outcomes of the light curve solutions, Figure 2 shows corner plots of the systems in the MCMC modeling, and Figure 3 displays the binary systems' observed and final synthetic light curves. Three-dimensional (3D) views of the binary systems and the starspots on the stars are shown in Figure 4. The color in Figure 4 represents the effective temperature variations on the surface of the stars (Paki et al. 2023).

[16] https://gea.esac.esa.int/archive/

Table 3
Light Curve Solutions of the Target Binary Stars

Parameter	TIC 249064185	TIC 318015356	TIC 397984843	TIC 55522736
T_1 (K)	$6166^{+(57)}_{-(84)}$	$6531^{+(33)}_{-(24)}$	$6569^{+(47)}_{-(59)}$	$5547^{+(60)}_{-(48)}$
T_2 (K)	$6050^{+(79)}_{-(42)}$	$6498^{+(24)}_{-(26)}$	$6417^{+(45)}_{-(55)}$	$5508^{+(52)}_{-(69)}$
$q = M_2/M_1$	$8.720^{+(421)}_{-(450)}$	$0.144^{+(1)}_{-(1)}$	$2.799^{+(7)}_{-(8)}$	$0.135^{+(9)}_{-(7)}$
i°	$70.15^{+(9)}_{-(11)}$	$85.92^{+(1)}_{-(1)}$	$83.67^{+(1)}_{-(1)}$	$83.11^{+(1)}_{-(1)}$
f	$0.538^{+(42)}_{-(45)}$	$0.691^{+(20)}_{-(11)}$	$0.254^{+(5)}_{-(7)}$	$0.603^{+(24)}_{-(37)}$
$A_1 = A_2$	0.5	0.5	0.5	0.5
$g_1 = g_2$	0.32	0.32	0.32	0.32
$\Omega_1 = \Omega_2$	13.259 (350)	2.022(65)	6.192(157)	2.009(53)
l_1/l_{tot}(TESS)	0.142(4)	0.839(7)	0.302(5)	0.850(5)
l_2/l_{tot}(TESS)	0.858(6)	0.161(5)	0.698(6)	0.150(4)
$l_1/l_{tot}(G)$	0.145(4)	0.840(7)	0.308(5)	0.851(5)
$l_2/l_{tot}(G)$	0.855(6)	0.160(5)	0.692(6)	0.149(4)
$r_{(mean)1}$	0.235(19)	0.576(12)	0.311(17)	0.577(15)
$r_{(mean)2}$	0.586(17)	0.259(15)	0.488(16)	0.250(19)
Phase shift(TESS)	+0.005(1)	+0.042(2)	−0.011(2)	−0.023(2)
Col.°(spot)	107	⋯	⋯	⋯
Long.°(spot)	302	⋯	⋯	⋯
Radius°(spot)	13	⋯	⋯	⋯
T_{spot}/T_{star}	0.89	⋯	⋯	⋯
Component	Secondary	⋯	⋯	⋯

4. Absolute Parameters

One of the main objectives of studies on contact binary systems will be to estimate the absolute parameters. Studying the evolution of stellar binary systems involves an appropriate standard of accuracy to estimate absolute parameters such as mass, radius, and luminosity. Using the Gaia DR3 parallax yields more accurate results to estimate absolute parameters (Li et al. 2021; Poro et al. 2024b, 2024c). In this estimation method, observational parameters such as orbital period P and apparent magnitude V, light curve solution results (q, $l_{1,2}/l_{tot}$, $r_{(mean)1,2}$, T_1, T_2), and Gaia DR3 parallax are used. We used $l_{1,2}/l_{tot}$ of G filter from the light curve solutions. Also, the V magnitude of each system comes from the TIC database for the calculations. The process of calculations and equations used is as follows, respectively (Equations (1)–(8)).

$$M_{V(system)} = V - 5\log(d) + 5 - A_V, \quad (1)$$

$$M_{V(1,2)} - M_{V(tot)} = -2.5\log(\frac{l_{(1,2)}}{l_{(tot)}}), \quad (2)$$

$$M_{bol} = M_V + BC, \quad (3)$$

$$M_{bol} - M_{bol_\odot} = -2.5\log\left(\frac{L}{L_\odot}\right), \quad (4)$$

$$R = \left(\frac{L}{4\pi\sigma T^4}\right)^{1/2}, \quad (5)$$

$$a = \frac{R}{r_{mean}}, \quad (6)$$

$$\frac{a^3}{G(M_1 + M_2)} = \frac{P^2}{4\pi^2}, \quad (7)$$

$$g = G_\odot\left(\frac{M}{R^2}\right). \quad (8)$$

We calculated the extinction coefficient (A_V) value using the 3D dust-map Python package considering the Gaia DR3 reported distance (Green et al. 2019). The Flower (1996) study was utilized to compute the bolometric correction (BC) throughout the estimating process.

Reasonable estimated absolute parameters using Gaia DR3 parallax require a low A_V value (Poro et al. 2024f). We obtained the absolute parameters using another method to ensure the validity of the estimations since the A_V of the TIC 249064185, TIC 318015356, and TIC 397984843 systems is large (Table 4). So, we used the orbital period and semimajor axis empirical relationship that was updated by the Poro et al. (2024f) study (Equation (9)).

$$a = (0.372^{+0.113}_{-0.114}) + (5.914^{+0.272}_{-0.298}) \times P. \quad (9)$$

Then, we used the mass ratio and Kepler's well-known third law equation to estimate the mass and uncertainty of each star (Equations (10) and (11)).

$$M_1 = \frac{4\pi^2 a^3}{GP^2(1 + q)}, \quad (10)$$

$$M_2 = q \times M_1. \quad (11)$$

The radius of the stars was estimated using $r_{mean1,2}$ (Equation (6)). Then the L, M_{bol}, and $\log(g)$ are possible to calculate using astrophysical equations.

The orbital angular momentum (J_0) of the systems was calculated for both estimation methods using Equation (12), which we referenced from the Eker et al. (2006) study

$$J_0 = \frac{q}{(1 + q)^2}\sqrt[3]{\frac{G^2}{2\pi}M^5 P}, \quad (12)$$

where q is the mass ratio, M is the total mass of the system, P is the orbital period, and G is the gravitational constant.

The results of estimating the absolute parameters for the four systems using Gaia DR3 parallax and P–a methods are listed in Table 4.

5. Discussion and Conclusion

We presented the first in-depth light curve solutions and estimations of the absolute parameters of four contact binary stars. We employed the TESS and Gaia survey observations of these binary systems for this investigation.

The light curve solutions show that the lowest effective temperature difference between the two stars is 33 K for TIC

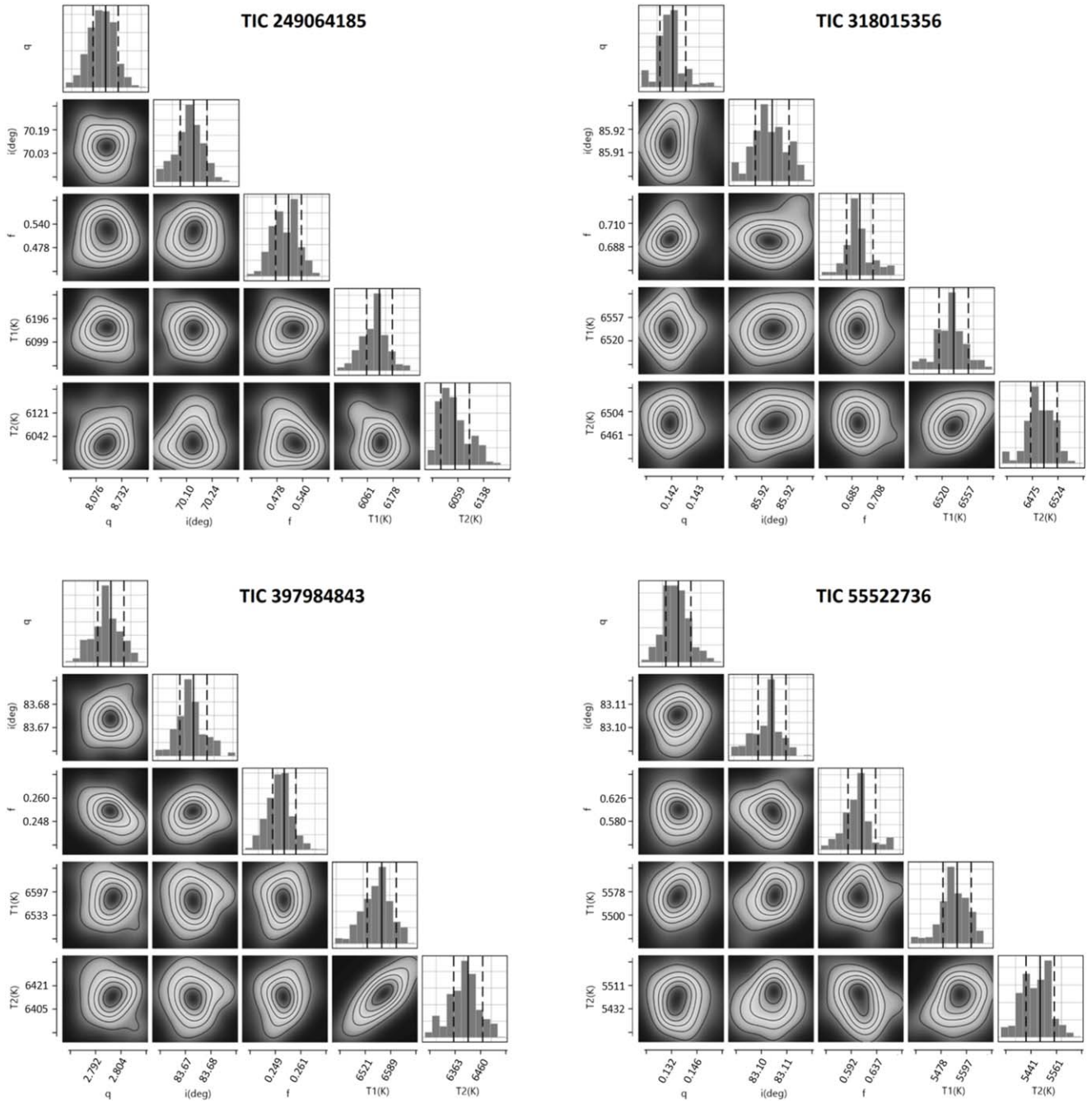

Figure 2. The corner plots of the target systems were determined by MCMC modeling.

318015356, and the highest is 152 K for TIC 397984843 (Table 5). The spectral category of the stars of the systems is also presented in Table 5 based on the Cox (2000) and Eker et al. (2018) studies.

We used the q-search method for photometric space-based data for target systems with total eclipses. TIC 249064185, TIC 318015356, and TIC 55522736, with respective mass ratios of $1/q = 0.115$, $q = 0.144$, and $q = 0.135$, are on the border of systems with extremely low-mass ratios (Li et al. 2024). Low-mass ratio contact binary systems ($q \leqslant 0.25$) have been the subject of investigations, and many questions remain (Li et al. 2022, 2024). Knowledge of the merging process and low-mass ratio limit depends on studies of contact binaries with low-mass ratios.

We employed two methods for estimating absolute parameters. First, the Gaia DR3 parallax was used for this estimation (Poro et al. 2024b, Table 4). The method of using parallax from

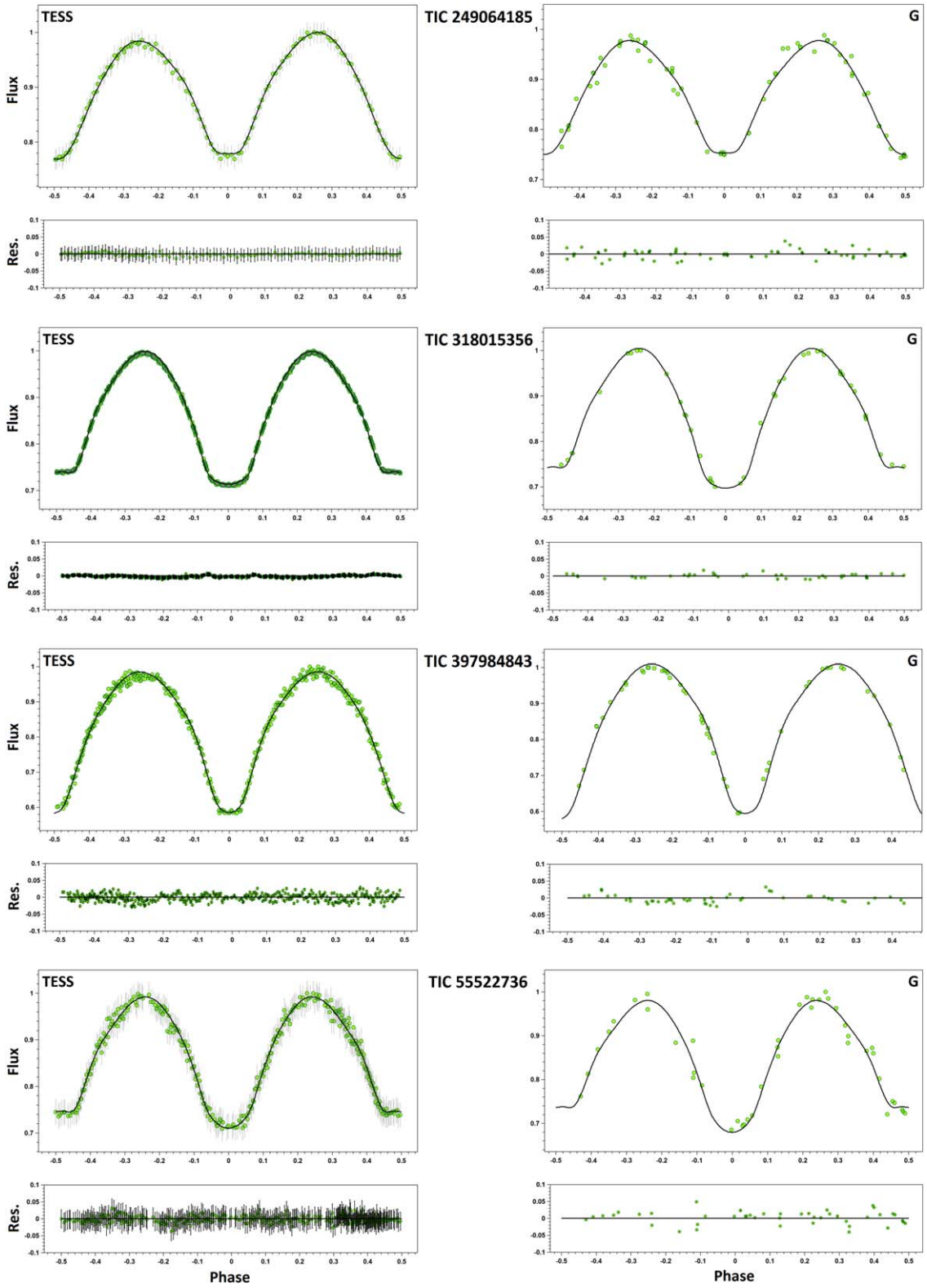

Figure 3. The green dots show the observed light curves of the systems, and the synthetic light curves were generated using the light curve solutions. The right side is the Gaia data, and the left side is the TESS data with their theoretical fits.

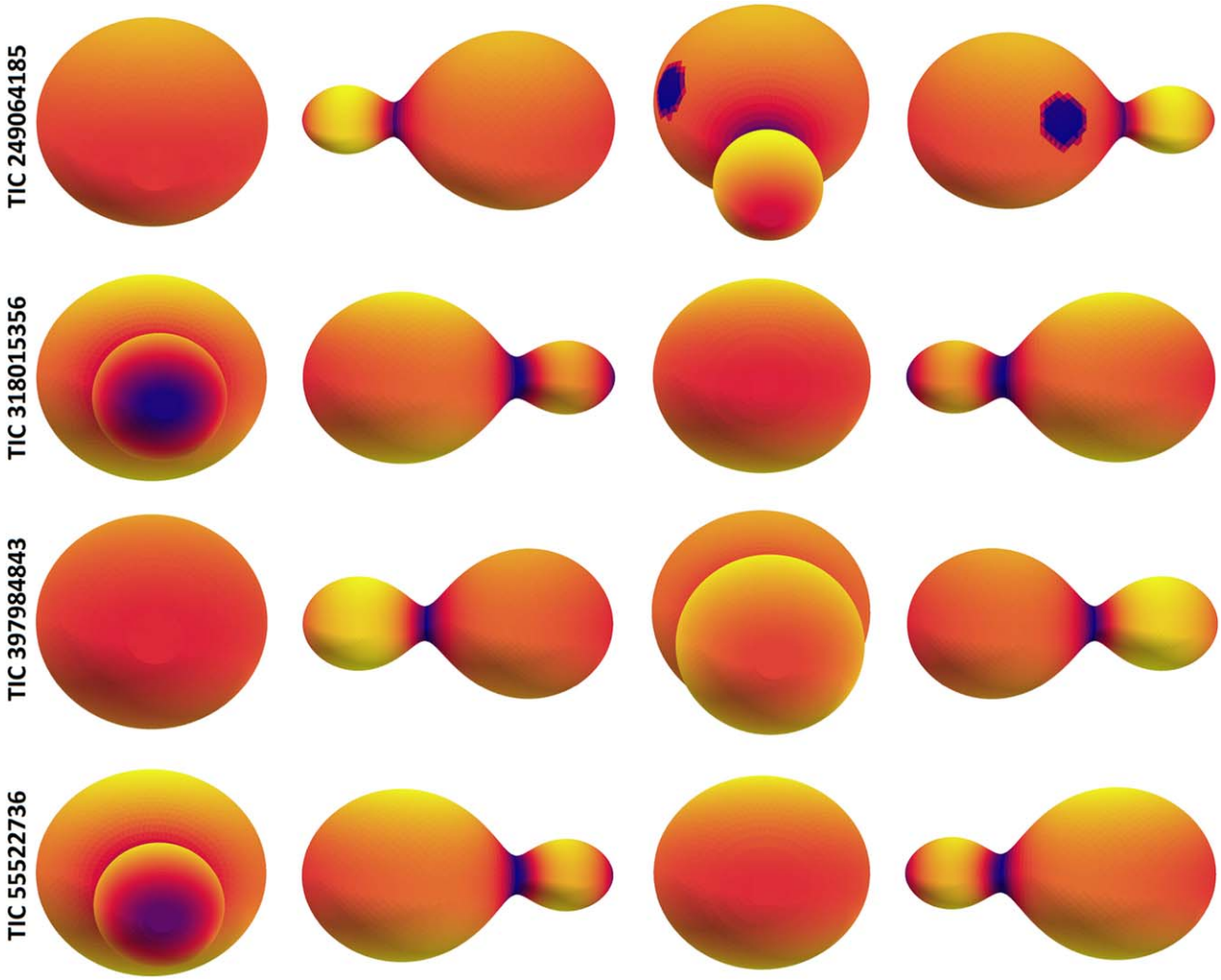

Figure 4. 3D view of stars in the four target binary systems in phases 0, 0.25, 0.5, and 0.75, from left to right respectively.

Gaia DR3 is accurate if the restrictions are observed. Using this method requires that the A_V value be low (Poro et al. 2024f). TIC 249064185, TIC 318015356, and TIC 397984843 have big A_V values, so doubts about the results of this method may arise, although A_V is carefully calculated. On the other hand, the difference in calculating the semimajor axis in the Gaia DR3 parallax method is denoted as Δa (Poro et al. 2024d). Δa is the separation value from the primary star to the secondary star (a_1) and from the secondary star to the primary star (a_2). Calculations following the Gaia DR3 parallax method were done from the path of each star separately, and the $a_{1,2}$ values can be different. If Δa is less than 0.1, the results are acceptable, and it is also an indication of the accuracy of light curve solutions (Poro et al. 2024b). As shown in Table 5, Δa values of the target systems are less than 0.1. However, we also considered the P–a empirical relationship to calculate the absolute parameters.

According to the light curve solutions, all four systems exhibit a total eclipse. Also, light curve solutions and estimation of absolute parameters indicate that the systems are W UMa-type contact binaries. Contact systems can be divided into two subtypes, A and W (Binnendijk 1970). The more massive component is a hotter star in the A-subtype, and if the less massive component has a higher effective temperature, it is classified as a W-subtype. Therefore, the TIC 318015356 and TIC 55522736 systems belong to the A-subtype, while two systems, TIC 249064185 and TIC 397984843, are the W-subtype (Table 5).

There are three categories for fill-out factors of the contact binary systems: deep ($f \geqslant 50\%$), medium ($25\% \leqslant f < 50\%$), and shallow ($f < 25\%$) eclipsing contact binary stars (Li et al. 2022). According to the results of the fill-out factor in the light curve solutions, there are three target systems of deep type and

Table 4
Estimated Absolute Parameters of the Systems by Two Methods

Parameter	TIC 249064185		TIC 318015356		TIC 397984843		TIC 55522736	
	Gaia DR3	*P–a*	Gaia DR3	*P–a*	Gaia DR3	*P–a*	Gaia DR3	*P–a*
$M_1(M_\odot)$	0.13(3)	0.16(5)	4.30(26)	1.54(41)	0.77(13)	0.49(13)	3.48(39)	1.49(41)
$M_2(M_\odot)$	1.16(22)	1.43(50)	0.62(4)	0.22(6)	2.16(37)	1.38(36)	0.47(5)	0.20(7)
$R_1(R_\odot)$	0.53(6)	0.57(10)	2.32(6)	1.63(17)	1.11(11)	0.96(13)	2.06(19)	1.54(17)
$R_2(R_\odot)$	1.35(16)	1.43(17)	1.03(1)	0.74(11)	1.75(18)	1.50(17)	0.88(7)	0.67(11)
$L_1(L_\odot)$	0.36(7)	0.43(19)	8.82(30)	4.38(1.06)	2.05(34)	1.54(52)	3.62(52)	2.04(58)
$L_2(L_\odot)$	2.18(44)	2.48(75)	1.68(2)	0.87(29)	4.66(82)	3.45(97)	0.64(8)	0.37(16)
M_{V1}(mag.)	5.86(19)	5.67(39)	2.37(4)	3.12(23)	3.95(18)	4.25(31)	3.47(14)	4.08(26)
M_{V2}(mag.)	3.93(21)	4.87(28)	4.17(1)	8.22(31)	3.07(19)	7.18(27)	5.36(12)	6.30(37)
$M_{\rm bol1}$(mag.)	5.84(20)	5.65(40)	2.38(4)	3.13(24)	3.96(18)	4.26(32)	3.34(16)	3.96(27)
$M_{\rm bol2}$(mag.)	3.90(22)	3.75(29)	4.18(1)	4.88(31)	3.07(19)	3.39(27)	5.23(14)	5.81(38)
$\log(g)_1$(cgs)	4.11(18)	4.14(3)	4.34(1)	4.20(2)	4.24(16)	4.17(1)	4.35(13)	4.24(1)
$\log(g)_2$(cgs)	4.24(19)	4.28(3)	4.21(1)	4.05(1)	4.29(16)	4.22(1)	4.22(12)	4.09(1)
$a(R_\odot)$	2.28(14)	2.44(21)	4.00(8)	2.84(23)	3.58(21)	3.08(24)	3.55(13)	2.68(23)
$M_{\rm tot}(M_\odot)$	1.29(25)	1.60(55)	4.92(29)	1.77(47)	2.93(51)	1.87(49)	3.95(44)	1.70(48)
$\log J_0(g\ {\rm cm^2\ s^{-1}})$	51.09(12)	51.25(20)	52.16(5)	51.42(17)	52.05(13)	51.72(17)	51.97(10)	51.36(20)
A_V(mag.)	0.504(4)		0.646(2)		1.169(9)		0.284(4)	
BC_1	−0.025(8)		0.008(2)		0.011(4)		−0.126(13)	
BC_2	−0.039(8)		0.006(2)		−0.001(4)		−0.135(15)	

Table 5
Some Conclusions Regarding the Target Systems

System	ΔT (K)	Sp.	Δa ($R_\odot$)	Subtype	$f_{\rm cat.}$	M_{1i} ($M_\odot$)	M_{2i} ($M_\odot$)	$M_{\rm lost}$ ($M_\odot$)	$t_{\rm system}$ (Gyr)
TIC 249064185	116	F8-G0	0.04	W	Deep	0.88	1.79	1.09	5.60
TIC 318015356	33	F3-F5	0.08	A	Deep	0.94	2.00	1.18	3.76
TIC 397984843	152	F3-F5	0.02	W	Medium	0.88	1.99	0.99	3.48
TIC 55522736	39	G8-G8	0.06	A	Deep	0.99	1.70	0.99	6.62

one system of medium type. We have displayed the fill-out factor category for each target system in Table 5.

In W UMa-type contact binary systems, understanding the initial mass of two components provides critical insights into their evolutionary processes. We calculated the initial masses of the primary (M_{1i}) and secondary (M_{2i}) components for the four contact binary systems using the method described by Yildiz & Doğan (2013). The reciprocal mass ratio ($1/q_i$) serves as a physical constraint to determine the initial masses of the components. So, the initial mass of the secondary star was estimated by Equation (13) (Yildiz & Doğan 2013)

$$\begin{aligned} M_{2i} &= M_2 + \Delta M \\ &= M_2 + 2.50(M_L - M_2 - 0.07)^{0.64}, \end{aligned} \tag{13}$$

where M_2 is the current mass of the secondary, and M_L is derived from the mass–luminosity relation (Equation (14)).

$$M_L = \left(\frac{L_2}{1.49}\right)^{\frac{1}{4.216}}. \tag{14}$$

We calculated the initial mass of the primary component using Equation (15)

$$\begin{aligned} M_{1i} &= M_1 - (\Delta M - M_{\rm lost}) \\ &= M_1 - \Delta M(1 - \gamma), \end{aligned} \tag{15}$$

where $M_{\rm lost}$ represents the mass lost in the system and γ is the ratio of $M_{\rm lost}$ to ΔM (Equation (16)).

$$M_{\rm lost} = \gamma \times \Delta M. \tag{16}$$

We set $\gamma = 0.664$ based on the Yildiz & Doğan (2013) results. Then we used the following equation from the Yıldız (2014) study to determine the ages of the four targets

$$t \approx t_{\rm MS}(M_{2i}) + t_{\rm MS}(\bar{M}_2), \tag{17}$$

$$\begin{aligned} t_{\rm MS} = &\frac{10}{(M/M_\odot)^{4.05}} \\ &\times(5.60 \times 10^{-3}\left(\frac{M}{M_\odot} + 3.993\right)^{3.16} + 0.042), \end{aligned} \tag{18}$$

where $\overline{M_2}$ is the average value of M_{2i} and M_L. The outcomes, including the initial masses of both stars, the mass loss, and the

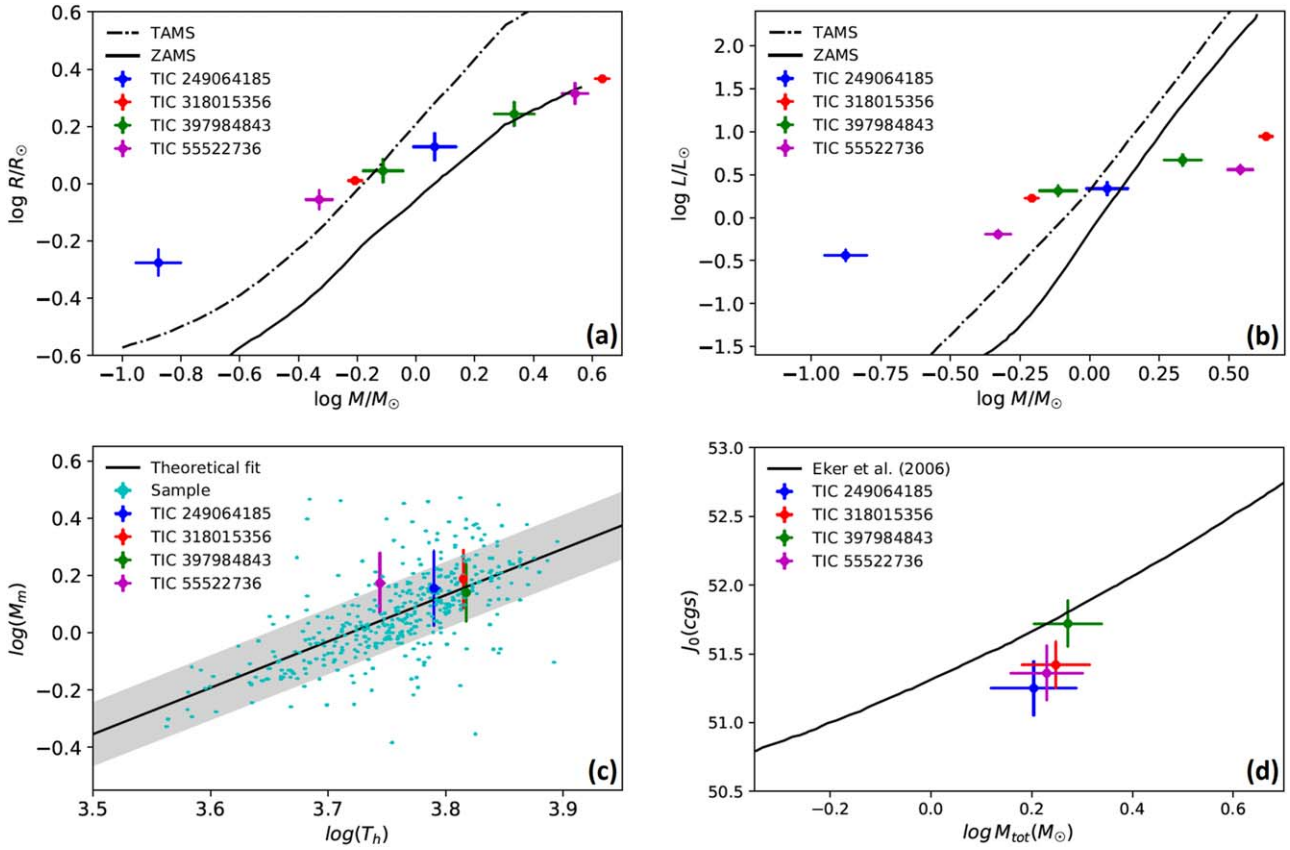

Figure 5. M–R, M–L, T_h–M_m, and $M_{\rm tot}$–J_0 diagrams.

systems' ages, are presented in Table 5. We found that these results are consistent with those reported by Yildiz & Doğan (2013) and Yıldız (2014).

Based on the estimation of absolute parameters, we displayed the evolution state of the systems on the Mass–Radius (M–R) and Mass–Luminosity (M–L) diagrams (Figure 5(a) and (b) respectively). The figures showed the star positions relative to the Terminal-Age Main Sequence (TAMS) and Zero-Age Main Sequence (ZAMS) lines from the Girardi et al. (2000) study.

The T_h–M_m relationship was presented by the Poro et al. (2024a) study using a sample of 428 contact binary systems. The more massive star was identified as M_m, and the hotter component as T_h. According to our results, we placed the star's position on the T_h–M_m diagram (Figure 5(c)). There is good agreement between the star locations and the fit of this empirical parameter relationship and its uncertainty.

We showed the location of each system in the $M_{\rm tot}$–J_0 diagram (Figure 5(d)) based on the results in Table 4. The area below the quadratic line in Figure 5(d) is associated with contact binary stars, whereas the area above represents detached systems. Consequently, four target systems are below the quadratic fit and in the contact binary region.

Acknowledgments

We have made use of data from the European Space Agency (ESA) mission Gaia (http://www.cosmos.esa.int/gaia), processed by the Gaia Data Processing and Analysis Consortium (DPAC, https://www.cosmos.esa.int/web/gaia/dpac/consortium). Funding for the DPAC has been provided by national institutions, in particular, the institutions participating in the Gaia Multilateral Agreement. This work includes data from the TESS mission observations. The NASA Explorer Program funds the TESS mission. This study uses information from the ASAS-SN variable star database. ASAS-SN was founded by the Gordon and Betty Moore Foundation through grants GBMF5490 and GBMF10501 to Ohio State University and the Alfred P. Sloan Foundation grant G-2021-14192. We thank Esfandiar Jahangiri for helping us in the study.

ORCID iDs

Atila Poro https://orcid.org/0000-0002-0196-9732
Razieh Aliakbari https://orcid.org/0009-0007-8508-2357
Hossein Azarara https://orcid.org/0009-0003-2631-6329
Asma Ababafi https://orcid.org/0009-0004-8579-7692
Sadegh Nasirian https://orcid.org/0009-0001-8140-1505

References

Binnendijk, L. 1970, VA, 12, 217
Borucki, W. J., Koch, D., Basri, G., et al. 2010, AAS Meeting Abstracts, 215, 101.01
Castelli, F., & Kurucz, R. L. 2004, A&A, 419, 725
Chen, X., Wang, S., Deng, L., et al. 2020, ApJS, 249, 18
Conroy, K. E., Kochoska, A., Hey, D., et al. 2020, ApJS, 250, 34
Cox, A. N. 2000, Allen's Astrophysical Quantities (New York: AIP Press; Springer)
Eker, Z., Bakış, V., Bilir, S., et al. 2018, MNRAS, 479, 5491
Eker, Z., Demircan, O., Bilir, S., & Karataş, Y. 2006, MNRAS, 373, 1483
Flower, P. J. 1996, ApJ, 469, 355
Foreman-Mackey, D., Hogg, D. W., Lang, D., & Goodman, J. 2013, PASP, 125, 306
Girardi, L., Bressan, A., Bertelli, G., & Chiosi, C. 2000, A&AS, 141, 371
Green, G. M., Schlafly, E., Zucker, C., Speagle, J. S., & Finkbeiner, D. 2019, ApJ, 887, 93
Heinze, A. N., Tonry, J. L., Denneau, L., et al. 2018, AJ, 156, 241
Henden, A. A., Levine, S., Terrell, D., & Welch, D. L. 2015, AAS Meeting Abstracts, 225, 336.16
Jayasinghe, T., Kochanek, C. S., Stanek, K. Z., et al. 2018, MNRAS, 477, 3145
Jenkins, J. M., Twicken, J. D., McCauliff, S., et al. 2016, Proc. SPIE, 9913, 99133E
Kallrath, J., & Milone, E. F. 1999, Eclipsing Binary Stars: Modeling and Analysis (New York: Springer)
Kopal, Z. 1959, Close Binary Systems (London: Chapman & Hall)
Lazarević, O., Čeki, A., & Lazarević, S. 2021, ApJS, 254, 10
Li, K., Gao, X., Guo, D.-F., et al. 2024, A&A, 692, L4
Li, K., Gao, X., Liu, X.-Y., et al. 2022, AJ, 164, 202
Li, K., Xia, Q.-Q., Kim, C.-H., et al. 2021, AJ, 162, 13
Loukaidou, G. A., Gazeas, K. D., Palafouta, S., et al. 2022, MNRAS, 514, 5528
Lucy, L. B. 1967, ZA, 65, 89
Lucy, L. B., & Wilson, R. E. 1979, ApJ, 231, 502
Marsh, F. M., Prince, T. A., Mahabal, A. A., et al. 2017, MNRAS, 465, 4678
O'Connell, D. 1951, MNRAS, 111, 642
Paki, E., Baudart, S., & Poro, A. 2023, Ap, 66, 452
Poro, A., Baudart, S., Nourmohammad, M., et al. 2024a, RAA, 24, 055001
Poro, A., Hedayatjoo, M., Nastaran, M., et al. 2024b, NewA, 110, 102227
Poro, A., Jafarzadeh, S. J., Harzandjadidi, R., et al. 2024c, RAA, 24, 025011
Poro, A., Li, K., Michel, R., et al. 2024d, AJ, 168, 272
Poro, A., Paki, E., Alizadehsabegh, A., et al. 2024e, RAA, 24, 015002
Poro, A., Tanriver, M., Michel, R., & Paki, E. 2024f, PASP, 136, 024201
Poro, A., Li, K., Paki, E., et al. 2025, MNRAS, 537, 3160
Prša, A., Conroy, K. E., Horvat, M., et al. 2016, ApJS, 227, 29
Ricker, G. R., Winn, J. N., Vanderspek, R., et al. 2015, JATIS, 1, 014003
Ruciński, S. M. 1969, AcA, 19, 245
Samus', N. N., Kazarovets, E. V., Durlevich, O. V., Kireeva, N. N., & Pastukhova, E. N. 2017, ARep, 61, 80
Sriram, K., Malu, S., Choi, C., & Rao, P. V. 2017, AJ, 153, 231
Taylor, M. B. 2005, in ASP Conf. Ser. 347, Astronomical Data Analysis Software and Systems XIV, ed. P. Shopbell, M. Britton, & R. Ebert (San Francisco, CA: ASP), 29
Yıldız, M. 2014, MNRAS, 437, 185
Yildiz, M., & Doğan, T. 2013, MNRAS, 430, 2029
Zhang, X.-D., & Qian, S.-B. 2020, MNRAS, 497, 3493